



HAL
open science

Evaluation of heat transfer correlations for HCCI engine modelling

H.S. Soyhan, H. Yasar, H. Walmsley, B. Head, G.T. Kalghatgi, C. Sorousbay

► **To cite this version:**

H.S. Soyhan, H. Yasar, H. Walmsley, B. Head, G.T. Kalghatgi, et al.. Evaluation of heat transfer correlations for HCCI engine modelling. Applied Thermal Engineering, 2008, 29 (2-3), pp.541. 10.1016/j.applthermaleng.2008.03.014 . hal-00498971

HAL Id: hal-00498971

<https://hal.science/hal-00498971>

Submitted on 9 Jul 2010

HAL is a multi-disciplinary open access archive for the deposit and dissemination of scientific research documents, whether they are published or not. The documents may come from teaching and research institutions in France or abroad, or from public or private research centers.

L'archive ouverte pluridisciplinaire **HAL**, est destinée au dépôt et à la diffusion de documents scientifiques de niveau recherche, publiés ou non, émanant des établissements d'enseignement et de recherche français ou étrangers, des laboratoires publics ou privés.

Accepted Manuscript

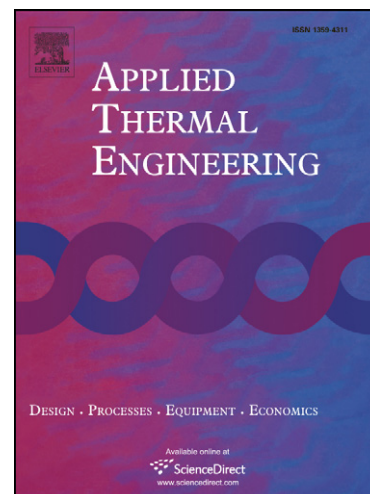
Evaluation of heat transfer correlations for HCCI engine modelling

H.S. Soyhan, H. Yasar, H. Walmsley, B. Head, G.T. Kalghatgi, C. Sorousbay

PII: S1359-4311(08)00155-5
DOI: [10.1016/j.applthermaleng.2008.03.014](https://doi.org/10.1016/j.applthermaleng.2008.03.014)
Reference: ATE 2449

To appear in: *Applied Thermal Engineering*

Received Date: 2 November 2007
Revised Date: 4 February 2008
Accepted Date: 10 March 2008



Please cite this article as: H.S. Soyhan, H. Yasar, H. Walmsley, B. Head, G.T. Kalghatgi, C. Sorousbay, Evaluation of heat transfer correlations for HCCI engine modelling, *Applied Thermal Engineering* (2008), doi: [10.1016/j.applthermaleng.2008.03.014](https://doi.org/10.1016/j.applthermaleng.2008.03.014)

This is a PDF file of an unedited manuscript that has been accepted for publication. As a service to our customers we are providing this early version of the manuscript. The manuscript will undergo copyediting, typesetting, and review of the resulting proof before it is published in its final form. Please note that during the production process errors may be discovered which could affect the content, and all legal disclaimers that apply to the journal pertain.

EVALUATION OF HEAT TRANSFER CORRELATIONS FOR HCCI ENGINE MODELLING

H.S.Soyhan^{1,2*}, H.Yasar^{1,2}, H.Walmsley¹, B.Head¹, G.T.Kalghatgi¹ and C.Sorusbay³

¹ Shell Global Solutions, Technology Centre Thornton, CH1 3SH, Chester, United Kingdom

² Dept. of Mechanical Engineering, Engineering Faculty, University of Sakarya, Turkey

³ Faculty of Mechanical Engineering, Technical University of Istanbul, Turkey

Abstract

Combustion in HCCI engines is a controlled auto-ignition of well-mixed fuel, air and residual gas. The thermal conditions of the combustion chamber are governed by chemical kinetics strongly coupled with heat transfer from the hot gas to the walls. The heat losses have a critical effect on HCCI ignition timing and burning rate, so it is essential to understand heat transfer process in the combustion chamber in the modelling of HCCI engines. In the present paper, a comparative analysis is performed to investigate the performance of well-known heat transfer correlations in an HCCI engine. The results from the existing correlations are compared with the experimental results obtained in a single cylinder engine. Significant differences are observed between the heat transfer results obtained by using Woschni, Assanis and Hohenberg correlations.

Key words: HCCI, Ricardo Hydra engine, modelling, heat transfer correlations

Nomenclature

* Correspondence to: Hakan S. Soyhan, Sakarya University, Engineering Faculty, Dept. of Mechanical Engineering, 54187, Esentepe-Sakarya, Turkey Tel.: +90 2642955854; Fax: +90 2642955601 (shared fax). E-mail address: hsoyhan@hotmail.com; hsoyhan@sakarya.edu.tr

Symbols

A_{head}	Cylinder head area (m ²)
A_{liner}	Cylinder liner area (m ²)
A_{piston}	Piston top area (m ²)
A_{head}	Cylinder head area (m ²)
B	Bore (m)
$h_g(t)$	Instantaneous gas-side heat transfer coefficient (w m ⁻² K ⁻¹)
$H(t)$	Instantaneous height of chamber (m)
$L(t)$	Instantaneous combustion chamber height (m)
n	Engine speed (rpm)
P	Instantaneous cylinder pressure (bar)
P_{int}	Intake manifold pressure (bar)
$P_{mot}(t)$	Instantaneous motored cylinder pressure (bar)
\dot{Q}	Instantaneous heat flux to the walls (kW)
\bar{s}_p	Mean piston speed (m s ⁻¹)
T	Instantaneous cylinder gas temperature (K)
T_{int}	Intake manifold temperature (K)
T_{w-head}	Instantaneous gas-side head-wall temperature (K)
$T_{w-liner}$	Instantaneous gas-side liner-wall temperature (K)
$T_{w-piston}$	Instantaneous gas-side piston-wall temperature (K)

V Instantaneous cylinder volume (m^3)

V_s Swept volume (m^3)

Greek symbols

v Gas velocity (m s^{-1})

γ Specific heats ratio

λ Excess air ratio

Abbreviations

abs Absolute

CAD Crank angle degree

CI Compression ignition

EGR Exhaust gas recirculation

EVC Exhaust valve closing time

EVO Exhaust valve opening time

HCCI Homogeneous charge compression ignition

int Intake

IVC Intake valve closing time

IVO Intake valve opening time

SI Spark ignition

1. Introduction

HCCI is a form of internal combustion in which well-mixed fuel and oxidizer are compressed to the point of auto-ignition. HCCI has characteristics of both of homogeneous charge spark ignition (SI) and stratified charge compression ignition (CI), and has the potential to combine their best properties. The fuel and oxidizer are mixed together as in SI engines but instead of an electric discharge to ignite the mixture, the pressure and temperature of the mixture are raised by compression until the entire mixture reacts simultaneously as in CI engines. The main characteristic of HCCI is the simultaneous burning of the fuel/air mixture because of ignition occurring at several places simultaneously. In recent years, a number of studies related to the HCCI combustion have been published [1-12].

The HCCI process essentially involves a premixed fuel/air mixture at equivalence ratios that are generally lean. Ignition leads to very rapid combustion where all heat is released approximately within 5-15 crank angle degree (CAD). In an effort to understand how mixture preparation and in-cylinder thermodynamic conditions affect the chemical kinetics, models of varying resolution provide a good basis for exploring the HCCI combustion phenomena.

The heat transfer from the bulk gas to the combustion chamber in HCCI engines is one of the most important and difficult tasks in HCCI simulations since it influences the in-cylinder pressure and temperature, the fuel consumption and the pollutants. In general,

detailed chemistry is always coupled to empirical models describing the heat transfer process in HCCI engines. Several papers have been published on gas-to-wall heat transfer process suggesting some correlations to calculate the heat transfer coefficient in SI and CI engines [13-17]. Woschni [14], Annand [15], and Hohenberg [16] are widely used correlations in heat transfer calculations.

In this paper, the heat transfer correlations mentioned above will be evaluated for an HCCI engine. Since forced convection from the bulk gas to the combustion chamber walls is the dominant heat transfer mechanism in an HCCI engine, the radiation effect will be neglected. The validity of these approaches will be investigated by experimental data obtained from the single HCCI Engine in Shell Global Solutions laboratories.

The paper is organized as follows. After the introduction, Section 2 introduces our engine model and reviews the existing heat transfer correlations; Section 3 gives the details of the experimental setup; Section 4 examines the calculated results by using the correlations and their comparison against the experiments; Section 5 presents conclusions. There are nomenclature and references complementing the paper.

2. Model and Correlations

2.1. The engine model

The model is based on the Shell SI engine code called TRICE¹. Several modifications were made to TRICE so that it could be used for HCCI engine modeling. SI TRICE uses a quasi-dimensional method with physically separate burnt and unburnt gas zones of defined geometry. Either a Wiebe function or a turbulent burning rate model can be used to specify how much burnt and unburnt gas exists at a given crank angle. The HCCI code uses the Wiebe function option since a turbulent flame model has no role in HCCI combustion. Also the spatial separation of burnt and unburnt gas has almost no relevance to HCCI and is dropped from the HCCI modification (e.g. separate heat loss calculations for burnt and unburnt gas zones are abandoned because the two zones are more intimately mixed and flame engulfment calculations based on a fixed flame geometry are no longer relevant.)

Pressures during expansion could be affected by mass losses due to blow-by, which was not included in the basic TRICE model. Therefore, TRICE was adapted to include a basic blow-by model by forcing the exhaust valve to open slightly during the expansion stroke. In this way blow-by was represented by an orifice mass-flow calculation between

¹ TRICE is a modified version of SPICE [25] (Simulated Petrol Internal Combustion Engine), which was originally derived from the MIT Quasi model

cylinder pressure and atmospheric pressure and both mass and enthalpy losses were accounted for.

The heat transfer from gas to the walls is formulated as

$$\dot{Q} = h_g \left[A_{head} (T_g - T_{w-head}) + A_{piston} (T_g - T_{w-piston}) + A_{liner} (T_g - T_{w-liner}) \right] \quad (1)$$

where \dot{Q} is instantaneous heat transfer to the walls, A_{head} , A_{piston} and A_{liner} are the head, piston top and cylinder liner areas, respectively, h_g is the heat transfer coefficient of the gas boundary layer, T_g , T_{w-head} , $T_{w-liner}$ and $T_{w-piston}$ are the instantaneous temperatures for gas, gas side head-wall, gas side piston-wall and gas side liner-wall, respectively.

2.2. Heat Transfer Correlations

As mentioned in the introduction, several correlations calculating the heat transfer coefficient in SI and CI engines have been published in the literature. Among these, the Woschni [14], Assanis [8], and Hohenberg [16] correlations are widely used for HCCI engine modelling.

The original Woschni heat transfer correlation is given as,

$$h_g(t) = \alpha_s B^{-0.2} P(t)^{0.8} T(t)^{-0.55} v(t)^{0.8} \quad (2)$$

where α_s is a scaling factor used for tuning of the coefficient to match a specific engine geometry, B is the bore (m), P and T are the instantaneous cylinder pressure (bar) and gas temperature (K), respectively. The instantaneous characteristic velocity, v , is defined as

$v = c_1 \bar{s}_p + c_2 \frac{V_s T_r}{P_r V_r} (P - P_{mot})$ where $P_{mot} = P_r (V_r/V)^\gamma$ is the motored pressure. In this expression, c_1 and c_2 are the constants that need to be adjusted depending on the specific engine type, \bar{s}_p is mean piston speed ($\text{m}\cdot\text{s}^{-1}$), V_s is swept volume (m^3), V_r , T_r and P_r are volume, temperature and pressure (m^3 , K, bar) evaluated at any reference condition, such as inlet valve closure, V is instantaneous cylinder volume (m^3) and γ is the specific heats ratio. The second term in the velocity expression allows for movement of the gases as they are compressed by the advancing flame. There seems to be some difficulty with this interpretation because the pressure difference, and therefore predicted gas movement, remains after all real gas movements due to combustion would have finished. This is not appropriate to HCCI conditions and causes over-prediction of heat transfer during HCCI combustion. With empirical fitting of cycle averaged heat transfers, this in turn leads to under-prediction during compression, and hence undesirable consequences regarding predicting ignition, when the model is incorporated into a thermo-kinetic cycle simulation.

A modified Woschni correlation for HCCI engine was suggested in reference [8] as follows,

$$h_g(t) = \alpha_s L(t)^{-0.2} P(t)^{0.8} T(t)^{-0.73} v_{tuned}(t)^{0.8} \quad (3)$$

where the characteristic velocity is tuned as $v_{tuned} = c_1 \bar{s}_p + \frac{c_2}{6} \frac{V_s T_r}{P_r V_r} (P - P_{mot})$. In equation

(3), L is instantaneous chamber height (m), c_1 and c_2 are the constants which are 6.18 and

0.0 for gas exchange, 2.28 and 0.0 for compression, and 2.28 and 3.24×10^{-3} for combustion and expansion duration.

Henceforth in this paper this correlation will be referred to as “*Assanis Correlation*”. The Assanis correlation has three differences from the original Woschni heat transfer correlation: the instantaneous chamber height is used as the characteristic length scale, the temperature exponent is modified to be 0.73, and c_2 is reduced to 1/6 of the original value.

The Hohenberg [16] heat transfer correlation is given as

$$h_g(t) = \alpha_s V(t)^{-0.06} P(t)^{0.8} T(t)^{-0.4} (\bar{s}_p + b)^{0.8} \quad (4)$$

where the calibration constants, α_s and b , are calculated and used as 130 and 1.4 by Hohenberg. This correlation will be referred to as the “*Hohenberg Correlation*”.

2.3. Generic Form of Heat Transfer Correlations

In order to compare the heat transfer correlations it would be useful to reduce them to a single generic form. The Woschni, Assanis and Hohenberg correlations for the heat transfer coefficient can all be written in a single generic form as,

$$h_g(t) = \alpha_s L(t)^{-j} P(t)^k T(t)^{-l} v(t)^m \quad (5)$$

The definitions of L and v differ between the correlations, as do the values of α_s , j and l . In dimensionless form, this generic correlation can be written as:

$$\frac{h_g(t)}{h^*} = \left[\frac{\alpha}{\alpha^*} \right] \left[\frac{1}{B^{j-j_w} P^{*k-k_w} T^{*l-l_w} \bar{s}_p^{*m-m_w}} \right] \times \left[\frac{L(t)}{L^*} \right]^{-j} \left[\frac{P(t)}{P^*} \right]^k \left[\frac{T(t)}{T^*} \right]^{-l} \left[\frac{v(t)}{v^*} \right]^m \quad (6)$$

where α^* , L^* , P^* , T^* and v^* are characteristic values for scale factor, length, pressure, temperature and velocity and $h^* = \alpha^* L^{*j} P^{*k} T^{*l} v^{*m}$ is a characteristic heat transfer coefficient and j^* etc are characteristic values for the exponents. For length and velocity, it is most obvious to choose the bore, B , and the mean piston speed, \bar{s}_p , as the characteristic values. For other factors we, arbitrarily, use the Woschni correlation as a benchmark, and hence for the scaling factor we use the Woschni value, α_w and for pressure and temperature we use the cycle-averaged Woschni values, \bar{P}_w and \bar{T}_w . The exponents k and m are both 0.8 in all three correlations so terms with the exponents $k-k_w$ and $m-m_w$ drop out. With these substitutions and eliminations, the following expression may be written:

$$\frac{h_g(t)}{h^*} = \left[\frac{\alpha_s}{\alpha_w} \right] \left[\frac{1}{B^{j-j_w} \bar{T}_w^{l-l_w}} \right] \left[\frac{L(t)}{B} \right]^{-j} \left[\frac{P(t)}{\bar{P}_w} \right]^k \left[\frac{T(t)}{\bar{T}_w} \right]^{-l} \left[\frac{v(t)}{\bar{s}_p} \right]^m \quad (7)$$

This expression may also be written using the mean length scale, temperature, pressure and speed values for the particular correlation. It is useful to do this as it allows separation of the factors that affect overall scaling of the heat transfer coefficients from those that only influence the shape of the heat transfer coefficient vs crank angle curve. This leads to:

$$\frac{h_g(t)}{h^*} = \left\{ \left[\frac{\alpha_s}{\alpha_w} \right] \left[\frac{1}{B^{j-j_w} \bar{T}_w^{l-l_w}} \right] \left[\frac{\bar{L}}{B} \right]^{-j} \left[\frac{\bar{P}}{\bar{P}_w} \right]^k \left[\frac{\bar{T}}{\bar{T}_w} \right]^{-l} \left[\frac{\bar{v}}{\bar{s}_p} \right]^m \right\} \times \left\{ \left[\frac{L(t)}{\bar{L}} \right]^{-j} \left[\frac{P(t)}{\bar{P}} \right]^k \left[\frac{T(t)}{\bar{T}} \right]^{-l} \left[\frac{v(t)}{\bar{v}} \right]^m \right\} \quad (8)$$

The terms in the first braces of Eq. (8) provide an overall scaling factor and the terms in the second braces control the shape of the curve as a function of crank angle. Within the generic form of Eq. (7), the correlations differ in the definitions of L/B and v/\bar{s}_p , scale factor α_s and the values of the powers j and l as outlined in Table 1. In this table, the different correlations are compared on the basis of the Woschni correlation in order to decouple effects of the parameters that affect shape from the effects of the parameters that only influence scaling. Thus in the generic Equation 5, since the Woschni correlation uses the bore, B , as the length scale, the Assanis correlation needs the length scale multiplied by the factor H/B in row 1 of Table 1.

From the values in Table 1, it can be noted that the following further simplifications are possible:

- The Woschni and Assanis values for α_s are numerically identical and the Hohenberg value is only slightly different. The same is true for the length scale exponent, j . In both cases, the difference between the Hohenberg values and the others has only a minor influence on calculated heat transfer coefficients, so α_s and j can be regarded, for all practical purposes, as identical between correlations. Consequently the terms in α_s/α_w and B^{j-j_w} can be omitted from Eqs. (7) and (8).
- The pressures and temperatures obtained with all correlations are fairly similar so the terms containing \bar{P}/\bar{P}_w and \bar{T}/\bar{T}_w are close to one and, to a first approximation, these can also be omitted from Eqs. (7) and (8).

Applying these simplifications, Eqs. (7) and (8) reduce to:

$$\frac{h_g(t)}{h^*} = \left[\frac{1}{\bar{T}_w} \right]^{l-l_w} \left[\frac{L(t)}{B} \right]^{-j} \left[\frac{P(t)}{\bar{P}_w} \right]^k \left[\frac{T(t)}{\bar{T}_w} \right]^{-l} \left[\frac{v(t)}{\bar{s}_p} \right]^m \quad (7a)$$

and

$$\frac{h_g(t)}{h^*} = \left\{ \left[\frac{1}{\bar{T}_w} \right]^{l-l_w} \left[\frac{\bar{L}}{B} \right]^{-j} \left[\frac{\bar{v}}{\bar{s}_p} \right]^m \right\} \left\{ \left[\frac{L(t)}{\bar{L}} \right]^{-j} \left[\frac{P(t)}{\bar{P}} \right]^k \left[\frac{T(t)}{\bar{T}} \right]^{-l} \left[\frac{v(t)}{\bar{v}} \right]^m \right\} \quad (8a)$$

Eq. (8a) now can be used to compare the correlations and understand where the differences among the correlations arise.

First we examined the overall scaling of the heat transfer coefficient (i.e. the terms in the first pair of braces). The values of these terms are listed in Table 2. The temperature term, $\bar{T}_w^{l-l_w}$, varies significantly between correlations whereas the other terms are relatively similar². The temperature influence arises because the reference temperature \bar{T}_w is fairly large (~800 K) and the exponent, l , varies considerably ($\sim \pm 0.25$) between correlations.

We now consider the shapes of the heat transfer coefficient vs crank angle curves.

There are four relevant contributions: $\left[\frac{L(t)}{\bar{L}} \right]^{-j}$, $\left[\frac{P(t)}{\bar{P}} \right]^k$, $\left[\frac{T(t)}{\bar{T}} \right]^{-l}$ and $\left[\frac{v(t)}{\bar{v}} \right]^m$.

² The temperature term appears odd because it is not a dimensionless quantity. This issue arises because the α_s scaling values have different dimensions in each correlation but the ratio α_s/α_w has been omitted because they are assigned the same numerical value, if we were to retain the ratio of the α_s values it would render the temperature term dimensionless without altering its numerical value.

The influences of length scale, pressure, velocity and temperature on the magnitudes and shapes of the correlations are displayed by plotting $[L(t)/\bar{L}]^j$, $[P(t)/\bar{P}]^k$, $[T(t)/\bar{T}]^l$ and $[v(t)/\bar{v}]^m$ as a function of crank angle for each of the correlations as seen in Figs. 1 to 4. The influence of the different scaling factors on the magnitudes of the heat loss can also be seen in Table 1.

It should be noted that the length scale power, j , is the same in the Woschni and Assanis correlations, and almost the same in the Hohenberg correlation. The small difference between the Hohenberg value and the others would only have a minor influence on calculated heat transfer coefficients as can be seen in Fig. 1, so j can be regarded, for all practical purposes as identical between the models. It would also be possible to eliminate the $(\pi/4)^{1/3}$ in the velocity term of the Hohenberg correlation by incorporating $(\pi/4)^{-1/3}$ into α_s/α^* .

The velocity power, m , has no effect on the shape of Hohenberg correlation since $c_1+(c_2 T_r)/\bar{s}_p$ is a constant value where $c_2 = b/T_r$. There is a significant difference between the shape of the velocity terms in the Woschni and Assanis correlations. The effect of the six times reduced c_2 constant is seen significantly in Fig. 2. The difference between the Woschni and Hohenberg velocity terms is even more pronounced as the Hohenberg term is constant throughout the cycle. Although the shape is similar to Woschni correlation, the magnitude obtained by Assanis is approximately 2.5 times lower compared to Woschni correlation.

The temperature power, l , varies considerably between the correlations. All values are negative so the term acts to suppress the peak in heat transfer coefficient that occurs at combustion TDC as a result of the other terms. The greater the magnitude of the temperature power, the stronger the suppression of the peak. Thus the temperature term suppresses the peak most for the Assanis model and least for the Hohenberg correlation with the Woschni correlation in the middle as seen in Fig. 3.

Fig. 4 shows the influence of pressure on the magnitudes and shapes of the correlations as a function of crank angle for each of the correlations. It is seen here that Woschni and Assanis correlations gives almost same profile with some small differences in their magnitude while the trace obtained by using Hohenberg correlation is different in magnitude and shape together.

3. Experimental

3.1 The test engine

The engine used in this study is a Ricardo Hydra single-cylinder research engine with a Typhon 4-valve cylinder head with a pent roof. The piston has a raised crown to achieve the compression ratio of 14.04. In Table 3, the Ricardo Hydra engine specifications are presented along with the standard valve timings. There is no negative valve overlap with these valve timings hence minimal internal EGR.

The fuel was injected into the inlet port, targeted at the back of the closed inlet valves, close to the manifold. The timing of the fuel injection was at TDC of the compression stroke allowing the maximum amount of time for the fuel to be fully vaporized before induction into the cylinder. The cylinder pressure was measured with a Kistler 6125 piezoelectric pressure transducer located in the side of the pent-roof cylinder head. Heat release was calculated from the pressure signal.

The intake could be pressurized using an electrically driven compressor and intake air could be heated. The temperature of the fresh charge T_{int} was measured with a K thermocouple at a distance of 80 mm from the manifold head face, approximately 200 mm from the back of the inlet valve. A proportional–integral–derivative (PID) regulator held the charge temperature within 3 °C of the set temperature. The airflow was measured with a Cussons laminar air flow meter. The gravimetric fuel flow-rate was also measured. The mixture strength was measured by a Horiba MEXA 1500 exhaust gas analyzer, which delivers the excess air ratio, λ , and specific emissions data.

3.2 Experimental procedure

The engine operated at a constant lubricant and coolant temperatures of 90°C. Intake temperature, intake pressure, and engine speed were held constant and the fuel injection was adjusted until the chosen mixture strength, λ , was reached. An AVL data

acquisition system was used to analyse pressure data from 100 consecutive cycles on-line when combustion was stabilized.

Tests were done at the nominal intake pressure of 1.0 bar (abs) and the nominal intake temperature of 250 °C for λ values of 3.5, 4.0, 4.5 and 5.0. Engine speed was kept constant at 1200 rpm. An average pressure signal based on 100 cycles was also obtained and stored by the AVL system. In Table 4, the specifications of the fuel used during the current experiments are given.

4. Results and discussion

In this study, our target was to evaluate the three heat transfer coefficient models commonly being used in HCCI modeling. One of the most popular models, the Woschni correlation, is compared with the Assanis and Hohenberg correlations, although it was originally developed for CI engines conditions, which vary significantly from HCCI ones.

4.1 Results obtained from generic form

The original Woschni expression gives very high gas displacement velocities comparing to Assanis and Hohenberg expressions during combustion phase as seen in Figure 5. The maximum value reaches up to 35 m/s in Woschni expression, which is approximately 2.9 times more than Assanis and 7.6 times more than Hohenberg results. This is one of the reasons why Woschni expression gives very high heat transfer

coefficients. As seen in this figure, Hohenberg expression gives a constant gas displacement velocity for whole cycle. c_2 constant in the second term of the Woschni velocity expression is reduced by 6 times in the Assanis correlation since the high velocities resulting from the Woschni expression are not valid for HCCI particularly at low speeds (1200 rpm in our case). Figure 6 shows that heat transfer coefficient is reduced by approximately 50 % in the Assanis correlation while the shape looks very similar.

There are three different temperature powers, l , -0.4 , -0.55 and -0.73 used in the correlations. We used these three values in each correlation to see how the results would be affected. As seen in Fig. 7, the temperature power affects the level of heat transfer coefficient significantly. The Woschni correlation uses -0.55 as temperature power. If this is replaced by the Assanis value of -0.73 , the magnitude of the heat transfer coefficient becomes four times less than its original value while it is approximately 3 times more than its original value if the power of the temperature would be increased to -0.4 as it is in Hohenberg correlation. When we apply this type of comparison to the Assanis and Hohenberg correlations, the magnitude changes in a similar way but shapes do not change much with the variation of the temperature power.

While temperature power affects only the magnitude of the correlations, length scale factors affect both the magnitude and the shape of the correlations as seen in Fig. 8. The original Woschni heat transfer equation uses bore as length scale factor; it is instantaneous chamber height for Assanis and instantaneous cylinder volume for Hohenberg correlations. If the bore would be used as length scale factor in all three

correlations. Woschni keeps its characteristic shape and gives double the value in heat transfer coefficient value comparing to Hohenberg correlation while it is more than six times higher compared to Assanis correlation. The shapes are somehow similar to each other in all three correlations. If the instantaneous chamber height would be used as length scale factor in all three correlations Woschni keeps its characteristic shape with some changes in expansion stroke and gives almost triple the value in heat transfer coefficient compared to Hohenberg correlation while it is approximately more than ten times higher compared to Assanis correlation. The shapes are somehow similar to each other in Assanis and Hohenberg correlations. The most useful information in Fig. 8 appears in the Fig. 8c. When the length scale factor is changed in Woschni and Assanis to the instantaneous cylinder volume Woschni keeps its characteristic shape similar to the its original one with some changes in compression stroke and gives almost more than five times higher heat transfer coefficient value compared to Hohenberg and Assanis correlations. However, the shape obtained from Assanis by this changes becomes much more similar to the Hohenberg correlations but the peaks are both suppressed very much compared to Woschni correlation. This shows that the difference between Assanis and Hohenberg correlation is disappearing when the same length scale factor is used. They differ only in the magnitude, which can be easily adjusted by changing some of the constants. This figure also shows that the heat transfer coefficient calculation is very sensitive to the changes in length scale factors not only in magnitude but also in shapes.

4.2 Results obtained from parametric study

The validity of the correlations is checked also by comparing heat flux and the heat transfer coefficient traces for four mixture strengths, 3.5, 4.0, 4.5 and 5.0, at 1200 rpm. Fig. 9 shows the variation of the heat transfer coefficient calculated by the three correlations with absolute values on the first column and with the normalized values on the second column. The reason for giving the normalized traces as well is to have an easy comparison between the shape of the different traces since autoignition processes depend on the timing as well as the magnitude of heat losses. It is possible to vary the magnitude of heat losses by changing the scaling constants in the heat transfer correlations without changing the shape of the curves. The Assanis correlation gives very low absolute values but the shape is such that the peak heat loss is relatively high compared to the minimum. Thus when the losses are normalized with the mean values the Assanis curve has a higher peak than the Hohenberg correlation. Although this is shown only for $\lambda = 4.5$ value, this characteristic was the same for all λ values from 3.5 to 5. Similar behavior was also obtained for heat flux variation as seen in Fig. 10. Here the difference in shapes between the normalized values obtained by Assanis and Hohenberg correlations gets even closer to each other. They are almost same in intake, compression, expansion, and exhaust strokes while they differ in combustion duration by a factor of approximately 2. This difference was almost the same in normalized heat transfer coefficients traces given in Fig. 9, as well. This shows that there is a consistent trend in normalized shapes of heat transfer coefficient and heat flux.

It can be concluded from Figs. 9 and 10 that the normalized shapes obtained from the Hohenberg and Assanis correlations are almost the same but there are some magnitude differences which can be adjusted simply by engine or scaling parameters.

Cycle-average values of heat transfer coefficient and heat flux results are shown in Table 5. Table 6 gives ratios between cycle-maximum and cycle-average values for the heat transfer correlations to help comparing the different shapes.

The ratios of the maximum heat transfer coefficients given by different pairs of correlations for various mixture strengths in all strokes are given in Table 7. The highest ratio appears in combustion and expansion stroke as 6.39 times between Woschni and Assanis and 1.69 times between Woschni and Hohenberg correlations. Both the maximum values are obtained when λ is 3.5, and these ratios are reduced by increasing the excess air ratio. In other parts of the cycle the ratios are almost independent of mixture strength. These absolute differences change their characteristics when the heat transfer coefficients and the heat fluxes are normalized for each correlation by their own average values.

Pressure measurements were used for assessing Assanis and Hohenberg heat transfer correlations. Woschni is omitted from the presented data because of its unrealistic velocity term and high heat fluxes. Figs. 11 to 14 show the comparisons of the predicted and the experimental cylinder pressure curves for the mixture strengths of 3.5, 4.0, 4.5 and 5.0 at 1200 rpm. It can be clearly seen from the figures that the pressure curves obtained by

using the Hohenberg correlation match better against the experiments compared to the ones obtained by using the Assanis correlation. In all strokes except combustion, the results obtained by using Hohenberg correlation is almost identical with the measurements for all λ values while the curves by Assanis are slightly shifted up in all strokes. This difference gets less in richer conditions while λ values 3.5 and 4.0, and increases in higher λ values.

As a result, the Assanis correlation gives lower heat transfer coefficients compared to Hohenberg correlation and hence heat fluxes to the walls in the whole engine cycle. This under-prediction in engine heat transfer causes over-prediction in cylinder pressure. Although the differences in compression stroke are not so much between Assanis and measured data, small differences can have a strong impact on autoignition chemistry. Thus, small differences in compression stroke may cause big differences in subsequent heat loss which effects the end gas temperatures. Differences between predicted and measured pressure and temperature become more important in combustion stroke where the chemistry plays an important role.

5. Conclusions

In this work, an experimental and modeling work has been carried out to evaluate the performance of heat transfer correlations for HCCI engine modeling. The engine simulation code, TRICE, was modified and used to model the Ricardo Hydra single-cylinder research engine running on HCCI mode. Three common heat transfer correlations

were implemented into the model to evaluate their performance in comparison with the experimental data obtained in Shell Thornton.

At the end of the study, the following conclusions were reached. The Woschni correlation includes a term representing the combustion compression velocity, which is the bulk gas movement due to compression of the unburned gas by an advancing flame front. This representation is not applicable to HCCI engines, and leads to an unrealistically high gas velocity. Because of this, it exaggerates heat transfer rates during combustion and expansion and, if heat transfer rates are scaled to match measured cycle average heat losses, potentially underestimates heat transfer rates during compression. The Assanis correlation is a modified type of Woschni heat transfer correlation for HCCI engines that deals with gas movement issues empirically by reducing the magnitude of the combustion compression velocity. It gives very low heat transfer rates for whole engine cycle in our HCCI engine and consequently overestimates peak pressures. The Assanis model could be matched to our pressure data by adjusting the scaling coefficient. However, it is rather unsatisfactory to have to adjust coefficients substantially for each different HCCI engine. The Hohenberg heat transfer model, which has no explicit combustion compression velocity term, gives better agreement with our experiments than the other two models even without any empirical re-adjustment of the model coefficients.

Although there are differences in the magnitudes obtained by using Assanis and Hohenberg correlations, these could be easily eliminated by adjusting scaling constants.

However little adjustment is needed in Hohenberg constants, it is the simplest correlation and therefore it is advantageous to use Hohenberg correlations in HCCI simulations.

The heat transfer correlations discussed above will need to be modified specifically for HCCI combustion. The existing HCCI correlations are derived from SI correlations. HCCI processes are fundamentally different. It is likely that better correlations could be derived directly by making structural changes that represent more closely the nature of the HCCI process and not simply using empirical modifications to constants. Thus the combustion environment in HCCI engines would be better represented. The ultimate aim is to model the effect of combustion chamber deposits on the thermal environment of the engine and the consequent effects on HCCI combustion. These studies will be guided by existing experimental results.

Acknowledgements

This work has been financed under the European Commission Marie Curie Transfer of Knowledge Scheme (FP6) pursuant to Contract MTKI-CT-2004-509777 and was performed within a framework of a research and technological development program with the title SUSTAINABLE FUELUBE.

References

- [1] S. Onishi, S.H. Jo, K. Shoda, P.D. Jo, and S. Kato, Active Thermo-Atmosphere Combustion (ATAC) - A New Combustion Process for Internal Combustion Engines, SAE Paper 790501.
- [2] M. Noguchi, Y. Tanaka, T. Tanaka, and Y. Takeuchi, A Study on Gasoline Engine Combustion by Observation of Intermediate Reactive Products During Combustion, SAE paper 790840.
- [3] P.M. Najt, and D.E. Foster, Compression - Ignited Homogeneous Charge Combustion, SAE Paper 830264.
- [4] J. Bengtsson, P. Strandh, R. Johansson, P. Tunestål, and B. Johansson, Closed-Loop Combustion Control of Homogeneous Charge Compression Ignition (HCCI) Engine Dynamics, International Journal of Adaptive Control and Signal Processing, 18, pp. 167-179, 2004.
- [5] H.S. Soyhan, T. Lovas, and F. Mauss, A stochastic simulation of an HCCI engine using an automatically reduced mechanism, ASME Paper No: 2001-ICE-416, 2001; 37-2: 83-96.
- [6] S.M. Aceves, D.L. Flowers, F. Espinisco-Loza, A. Babajimopoulos, D.N. Assanis, Analysis of Premixed Charge Compression Ignition Combustion With a Sequential Fluid Mechanics-Multizone Chemical Kinetics Model, SAE paper 2005-01-0115.

[7] M. Sjober, J. Dec, N.P. Cernansky, “Potential of Thermal Stratification and Combustion Retard for Reducing Pressure-Rise Rates in HCCI Engines, Based on Multi-Zone Modeling and Experiments”, SAE paper 2005-01-0113.

[8] J. Chang, O. Guralp, Z. Filipi, D. Assanis, New Heat Transfer Correlation for An HCCI Engine Derived From Measurements of Instantaneous Surface Heat Flux, SAE paper 2004-01-2996.

[9] M. Konno, Z. Chen, Ignition Mechanisms of HCCI Combustion Process Fueled with Methane/DME Composite Fuel, SAE paper 2005-01-0182.

[10] S.M. Aceves, D.L. Flowers, C.K. Westbrook, J.R. Smith, R.W. Dibble, M. Christensen, W.J. Pitz, and B. Johansson, A Multi-Zone Model for Prediction of HCCI Combustion and Emissions, SAE Paper 2000-01-0327.

[11] D.L. Flowers, S. M. Aceves, J.R. Smith, J. Torres, J. Girard, R.W. Dibble, HCCI in a CFR Engine: Experiments and Detailed Kinetic Modeling, SAE Paper 2000-01-0328.

[12] R.W. Dibble, M.Au, J.W. Girard, S.M. Aceves, D.L. Flowers, and J.M. Frias, A Review of HCCI Engine Research: Analysis and Experiments, SAE Paper 2001-01-2511.

[13] K. Huber, G. Woschni, K. Zeilinger, Investigations on Heat Transfer in Internal Combustion Engines under Low Load and Motoring Conditions; SAE Paper 905018.

[14] G. Woschni, A Universally Applicable Equation for the Instantaneous Heat Transfer Coefficient in the Internal Combustion Engine; SAE Paper 670931.

[15] W. J. D. Annand and T. H. Ma, Instantaneous Heat Transfer Rates to the Cylinder Head Surface of a Small Compression-Ignition Engine, Proc. Instn. Mech. Engrs., 1970-1971; 185: 976-987.

[16] G. F. Hohenberg, Advanced Approaches for Heat Transfer Calculations; SAE Paper 790825.

[17] S. B. Han, Y. J. Chung, Y. J. Kwon and S. Lee, Empirical Formula for Instantaneous Heat Transfer Coefficient in Spark-Ignition Engine; SAE Paper 972995.

[18] D. Bradley, C. Morley and H. L. Walmsley, Relevance of Research and Motor Octane Numbers to the Prediction of Engine Autoignition; SAE 2004-01-1970.

Figure 1 Normalized characteristic length scale profiles

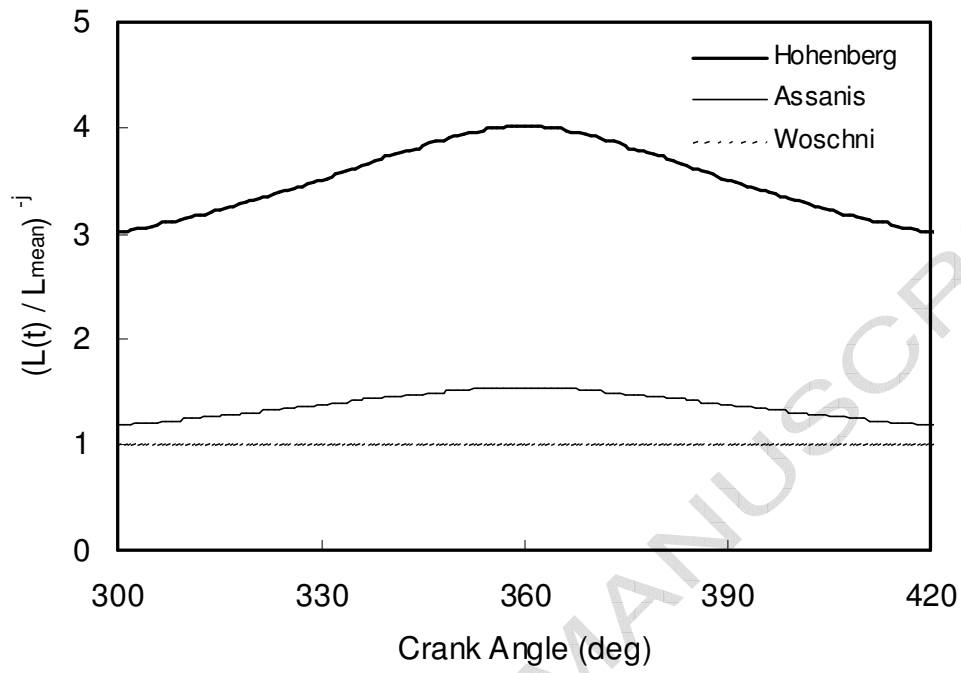


Figure 2 Normalized characteristic velocity profiles

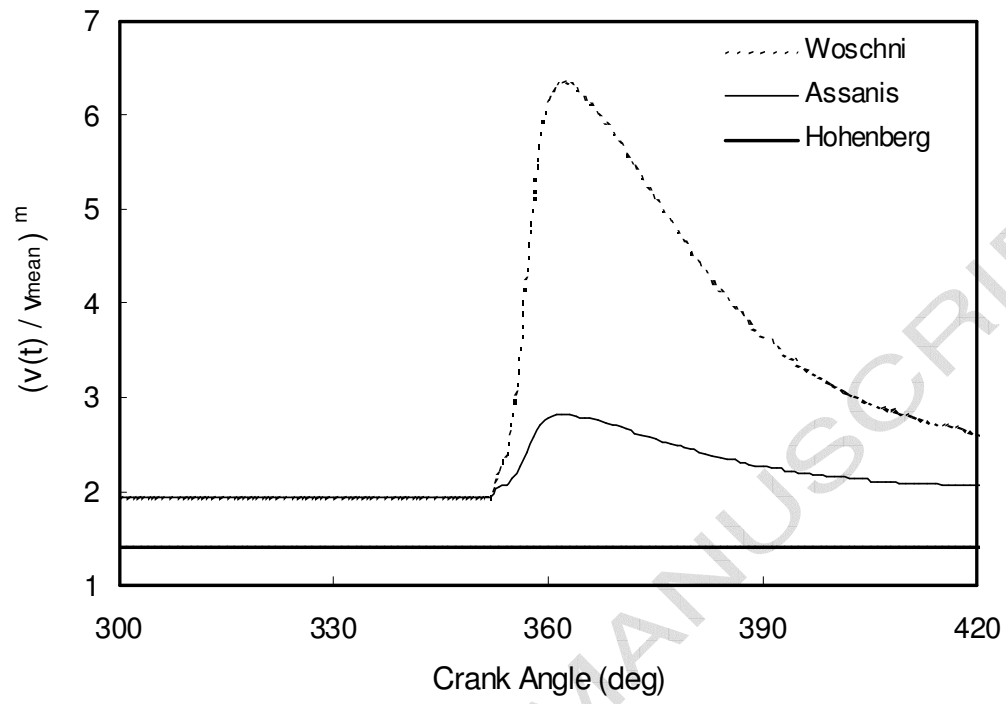


Figure 3 Normalized temperature profiles

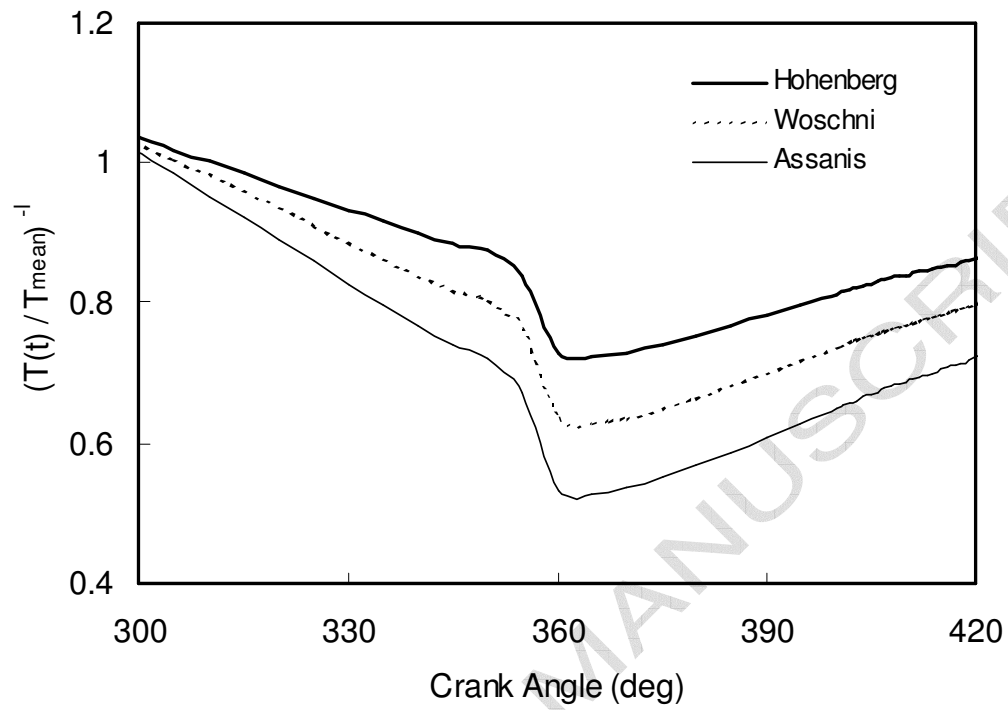


Figure 4 Normalized pressure profiles

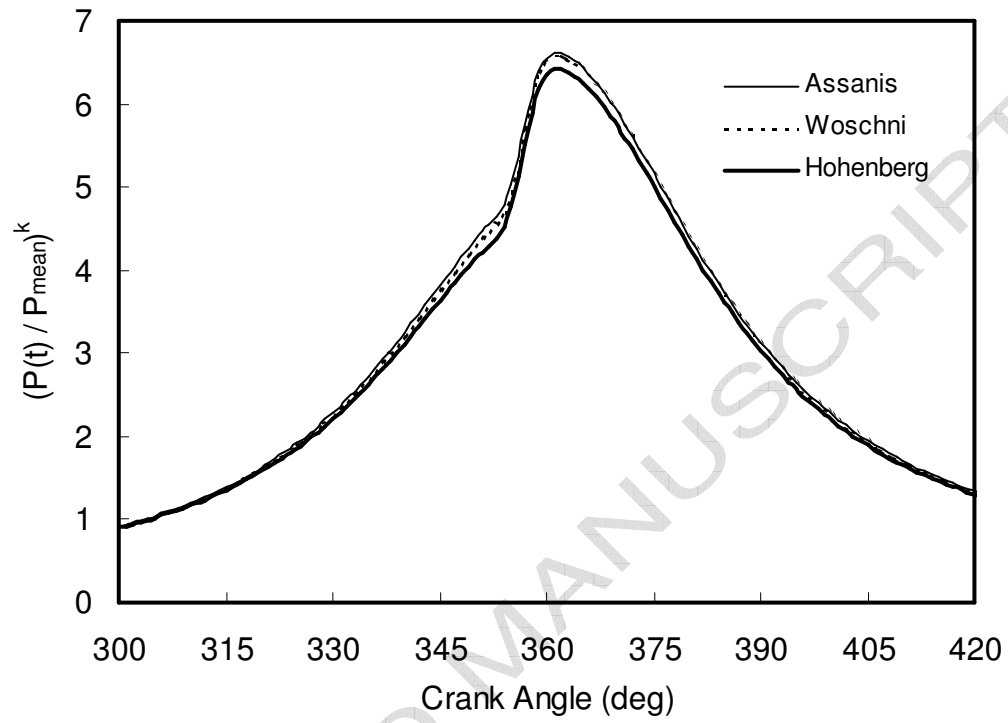


Figure 5 Variation of velocity term for each model

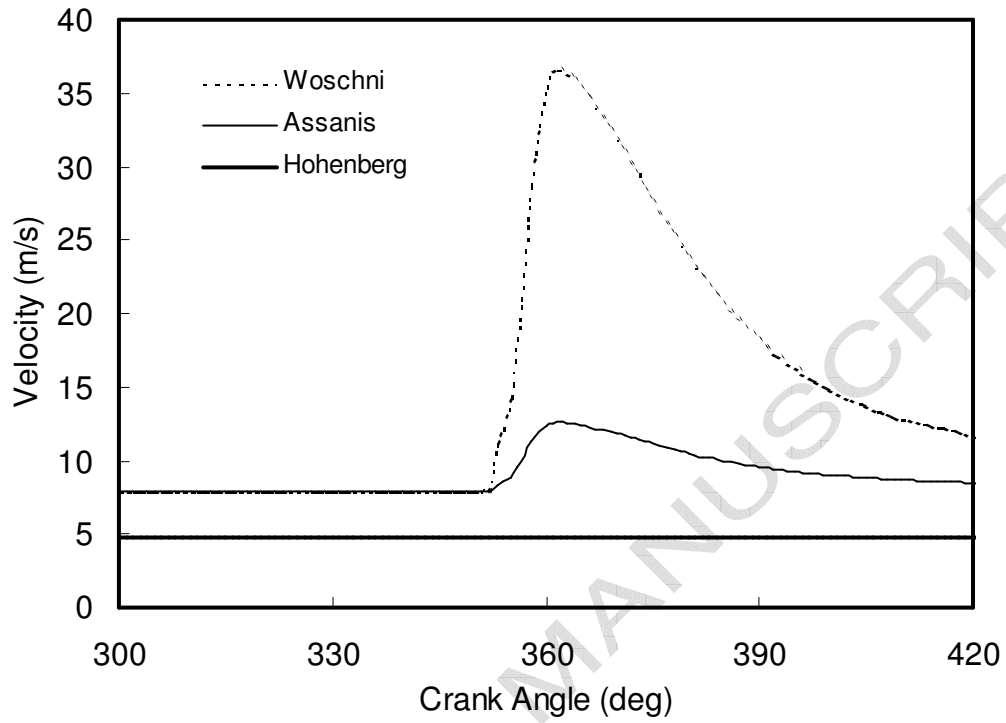


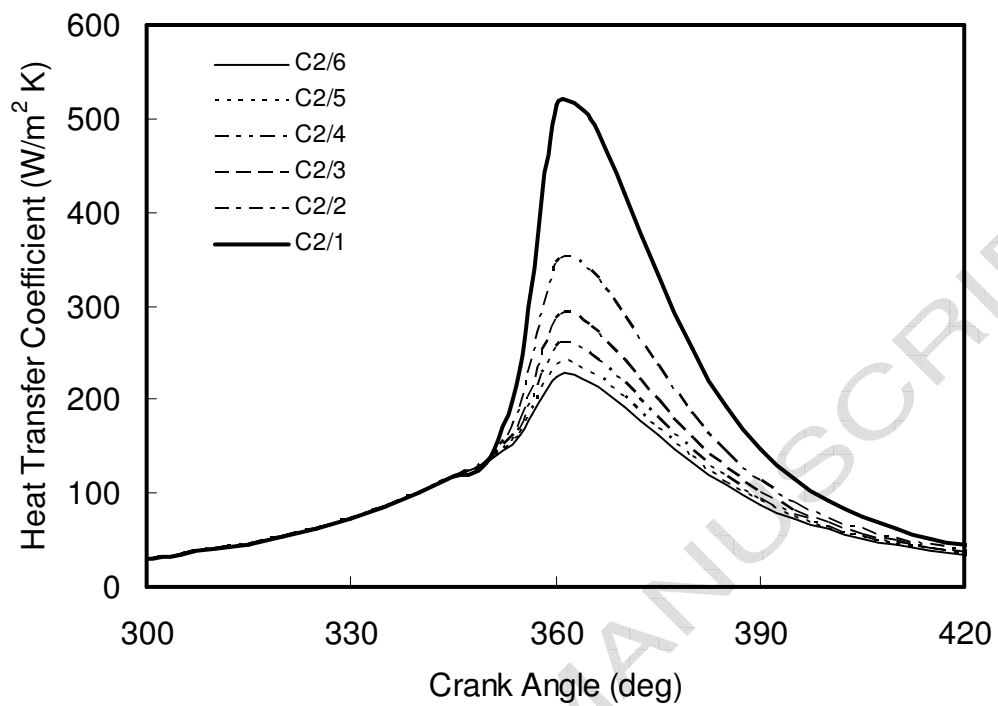
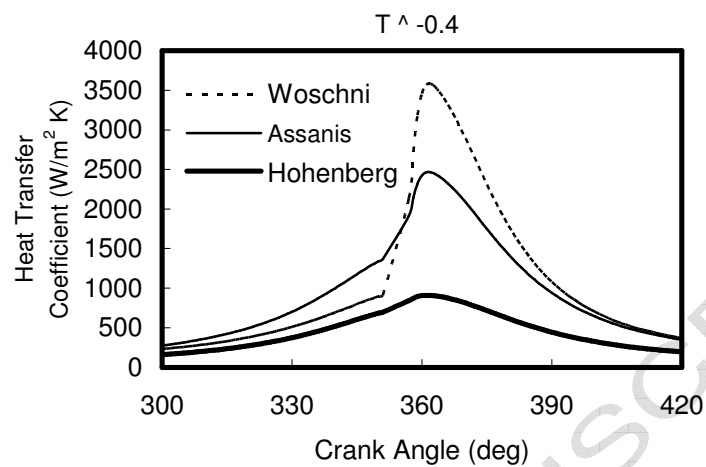
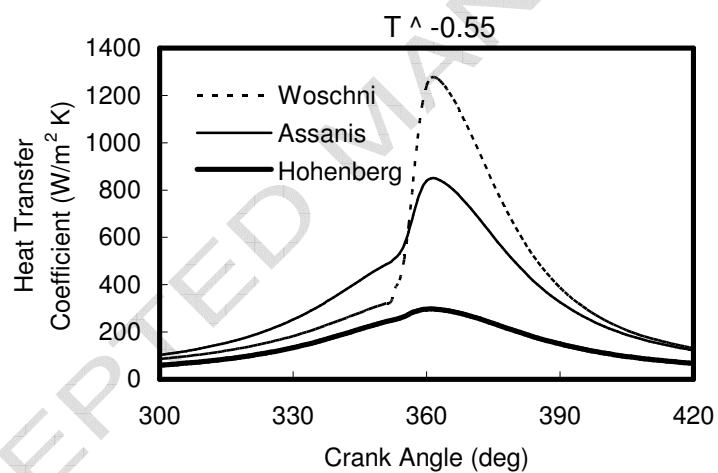
Figure 6 Effect of C_2 on heat transfer coefficient for Assanis model

Figure 7 Variation of heat transfer coefficient traces with different temperature exponents

A



B



34

C

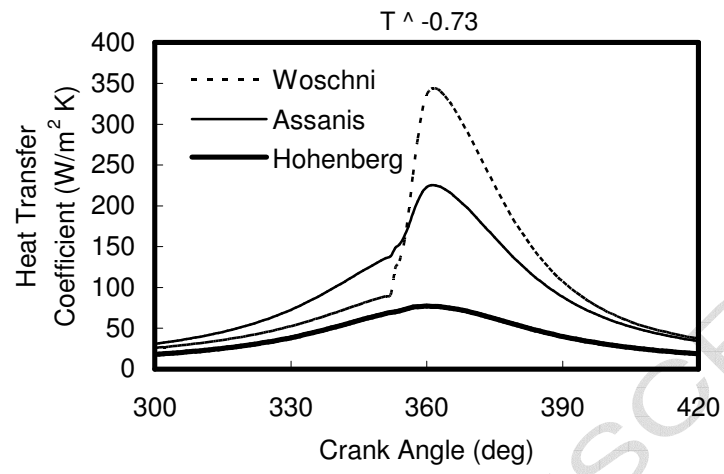
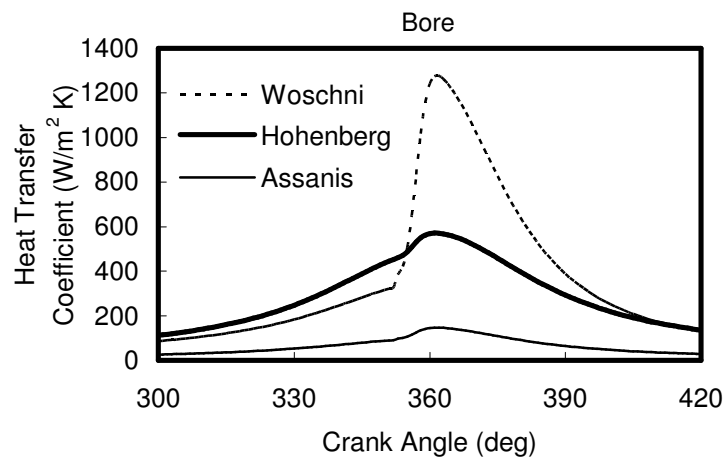
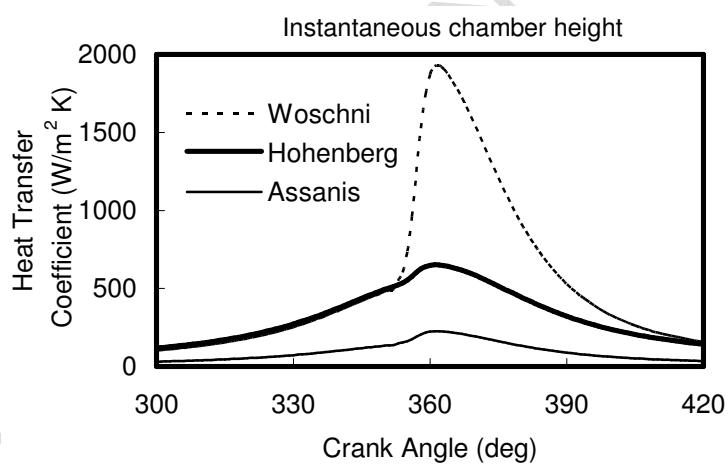


Figure 8 Variation of heat transfer coefficient traces with different length scale factors

A



B



36

C

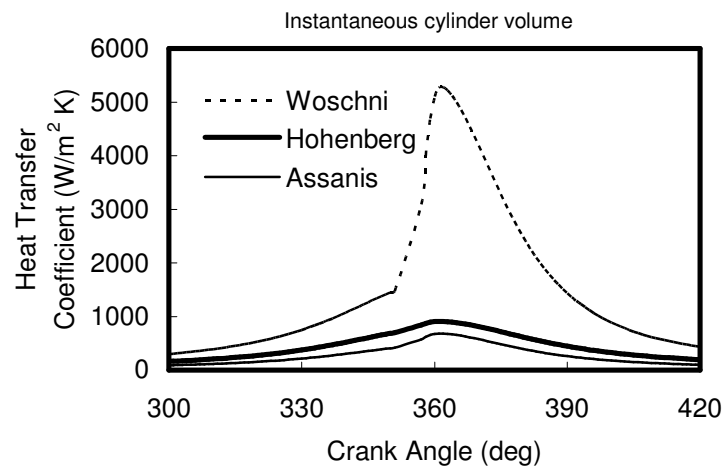
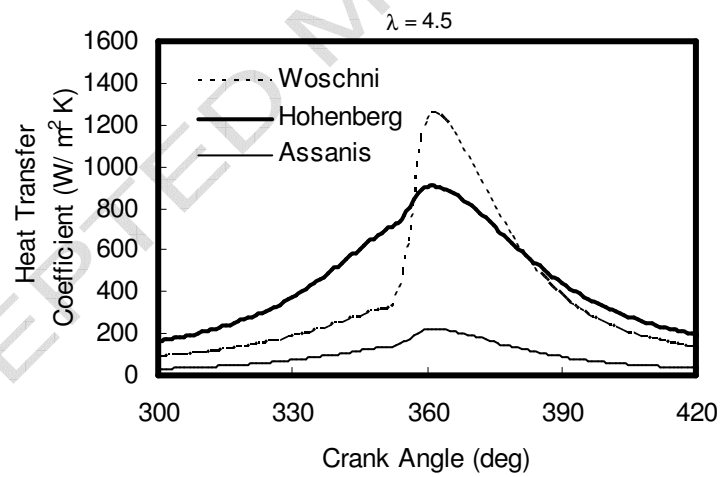


Figure 9 Heat transfer coefficient and cycle-averaged normalized heat transfer coefficient traces for different heat transfer models

A



B

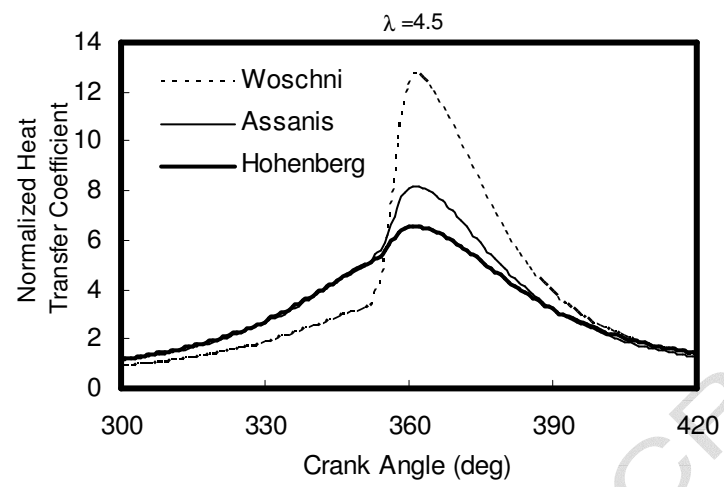
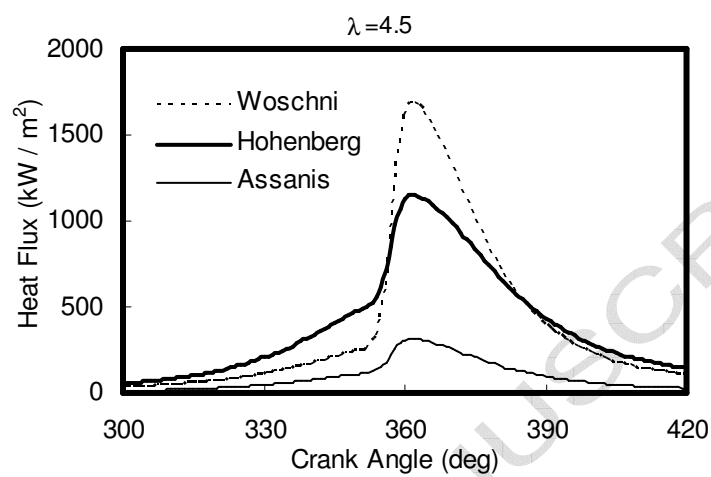


Figure 10 Heat flux and cycle-averaged normalized heat flux traces for different heat transfer correlations

A



B

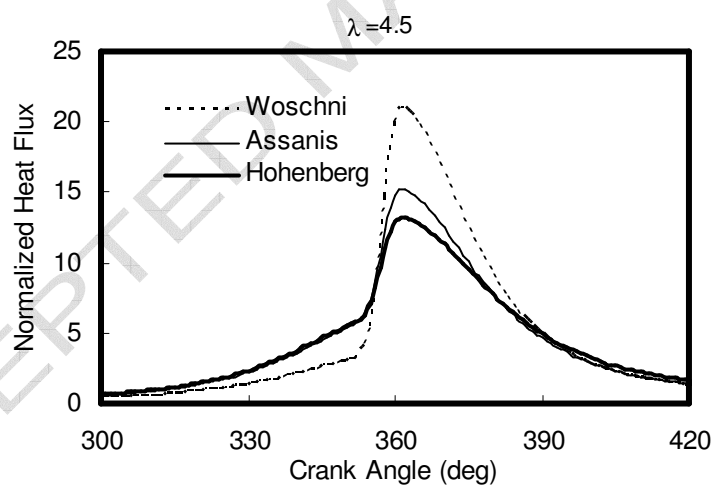


Figure 11 Measured and predicted cylinder pressure traces
($\lambda = 3.5$, $n = 1200$ rpm, $T_{\text{int}} = 523$ K, $P_{\text{int}} = 1.026$ bar, fuel = unleaded gasoline)

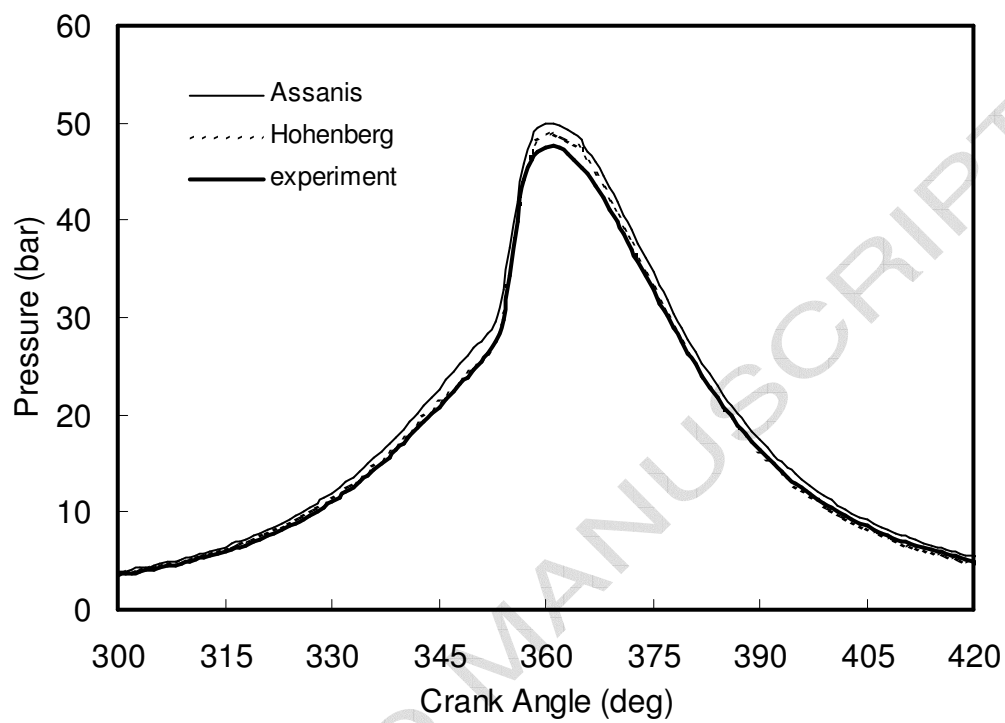


Figure 12 Measured and predicted cylinder pressure traces
($\lambda = 4.0$, $n = 1200$ rpm, $T_{\text{int}} = 523$ K, $P_{\text{int}} = 1.026$ bar, fuel = unleaded gasoline)

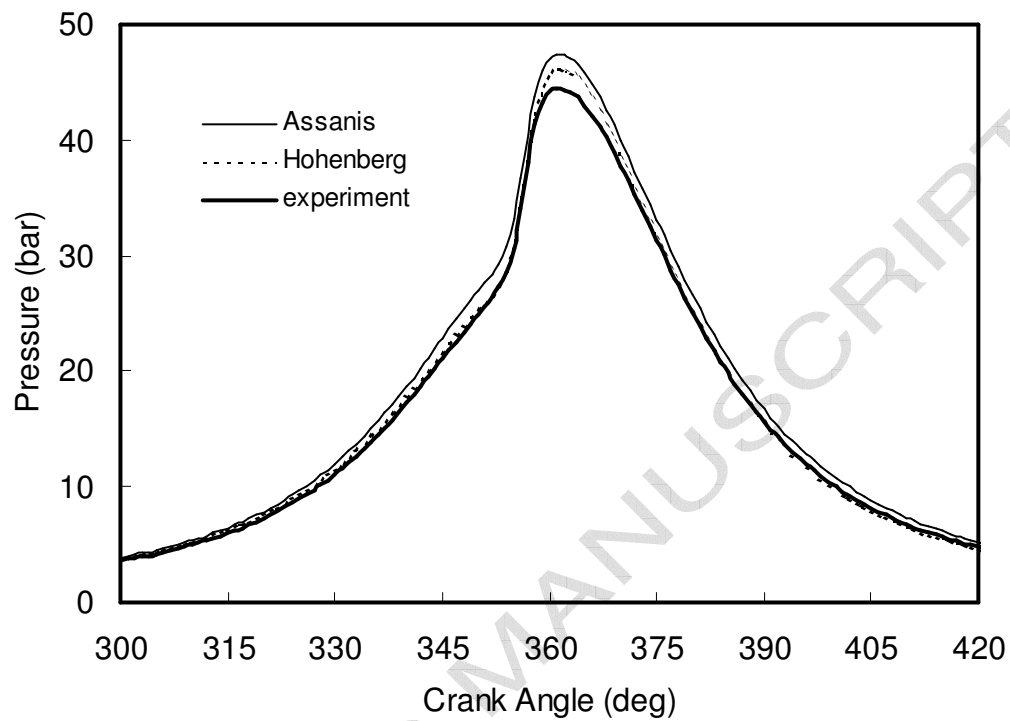


Figure 13 Measured and predicted cylinder pressure traces
($\lambda = 4.5$, $n = 1200$ rpm, $T_{\text{int}} = 523$ K, $P_{\text{int}} = 1.026$ bar, fuel = unleaded gasoline)

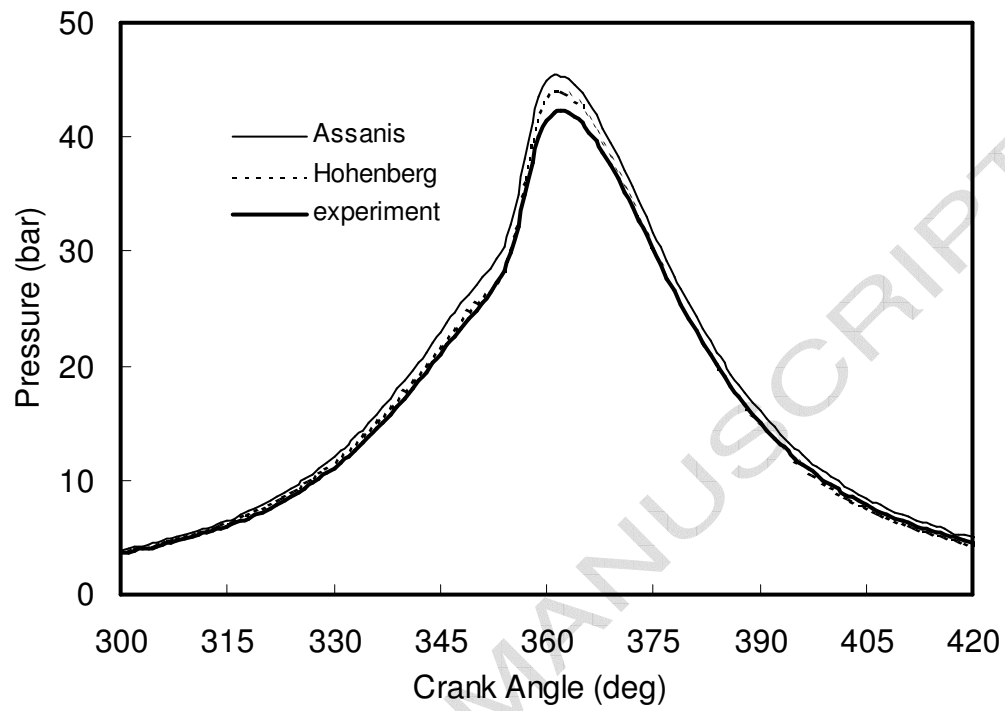


Figure 14 Measured and predicted cylinder pressure traces
($\lambda = 5.0$, $n = 1200$ rpm, $T_{int} = 523$ K, $P_{int} = 1.026$ bar, fuel = unleaded gasoline)

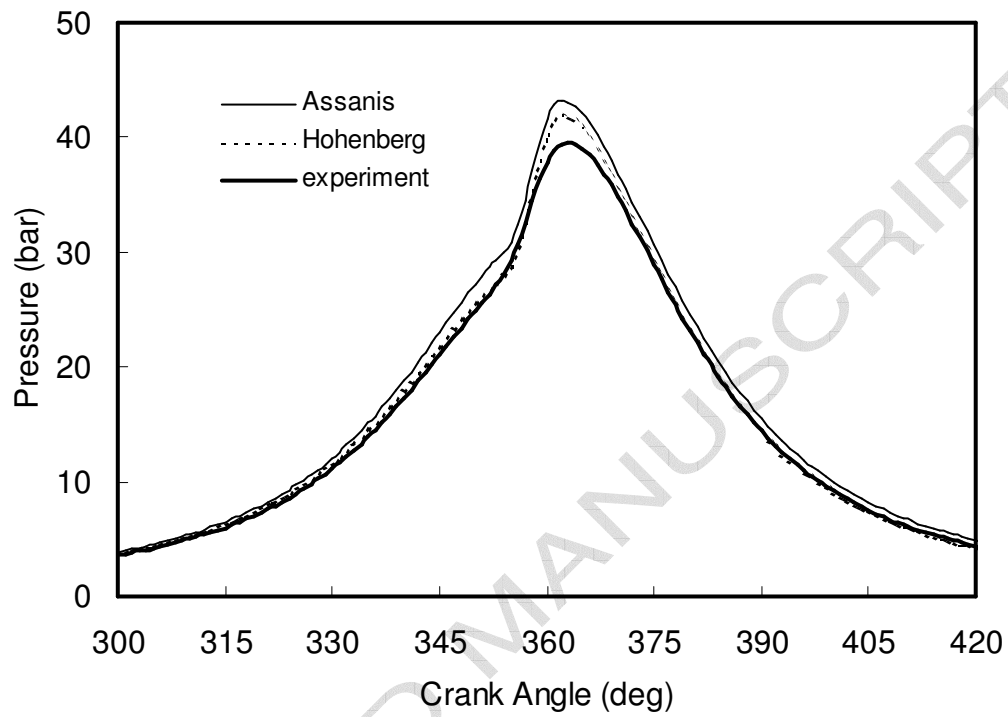


Table 1 Parameter definitions for each correlation

Parameter	Correlation		
	Woschni	Assanis	Hohenberg
L/L^*	1	$H(t)/B$	$(\pi/4)^{1/3}[H(t)/B]^{1/3}$
v/\bar{s}_p	$c_1(t) + \frac{c_2(t) V_s}{\bar{s}_p} \frac{(P(t) - P_{mol}(t))}{V_r} T_r$	$c_1(t) + \frac{c_2(t) V_s}{6\bar{s}_p} \frac{(P(t) - P_{mol}(t))}{V_r} T_r$	$c_1 + \frac{c_2 T_r}{\bar{s}_p}$, where $c_2 = b/T_r$
d/α^*	1	1	1.0
j	0.2	0.2	0.18
l	0.55	0.73	0.4
$c_1(t)$ in gas exchange	6.18	6.18	1
$c_1(t)$ in all other phases	2.28	2.28	1
$c_2(t)$ in gas exchange and compression	$0 \text{ m s}^{-1} \text{ K}^{-1}$	$0 \text{ m s}^{-1} \text{ K}^{-1}$	$b/T_r = 1.4/T_r$ $\text{m s}^{-1} \text{ K}^{-1}$
$c_2(t)$ in all other phases	$3.24 \times 10^{-3} \text{ m s}^{-1} \text{ K}^{-1}$	$3.24 \times 10^{-3} \text{ m s}^{-1} \text{ K}^{-1}$	$b/T_r = 1.4/T_r$ $\text{m s}^{-1} \text{ K}^{-1}$

Table 2 Terms influencing the overall scaling of the heat transfer coefficients

Description	Term		Correlation		
	Expression		Woschni	Assanis	Hohenberg
Temperature	$\left[\frac{1}{\overline{T}_w}\right]^{l-w}$		1.0	0.30	2.71
Length scale	$\left[\frac{\overline{L}}{\overline{B}}\right]^{-j}$		1.0	1.09	0.95
Speed	$\left[\frac{\overline{v}}{\overline{s}_p}\right]^m$		2.18	1.98	1.31
Combined	$\left[\frac{1}{\overline{T}_w}\right]^{l-w} \left[\frac{\overline{L}}{\overline{B}}\right]^{-j} \left[\frac{\overline{v}}{\overline{s}_p}\right]^m$		2.18	0.65	3.38

Table 3 Ricardo Hydra engine specifications [27]

Parameter	Value	Unit
Bore	86	mm
Stroke	86	mm
Connection rod length	143.5	mm
Compression ratio	14.04	-
Inlet valve diameter	32	mm
Number of valves	4	-
Inlet valve opening (IVO)	340	CAD
Inlet valve closing (IVC)	612	CAD
Exhaust valve opening (EVO)	120	CAD
Exhaust valve closing (EVC)	332	CAD

Table 4 The specifications of the fuel used during experiments [27]

Parameter	Value	Unit
Fuel Name	Unleaded gasoline	
Molecular Formula	$C_{6.43}H_{11.85}$	
RON	94.40	-
MON	84.00	-
Stoichiometric AFR.	14.53	-
Heat of combustion, ΔH	44.81	MJ kg ⁻¹
Density (at 20 °C)	0.731	g cm ⁻³

Table 5. Cycle-average values for heat transfer coefficient and heat flux

Excess air ratio λ	Cycle averaged values					
	Assanis		Hohenberg		Woshcni	
	h_g	\dot{Q}	h_g	\dot{Q}	h_g	\dot{Q}
3.5	38.08	27.42	140.86	102.17	144.73	117.22
4.0	37.67	25.03	139.37	93.68	136.55	98.76
4.5	37.38	23.46	138.37	87.53	131.36	86.90
5.0	37.09	21.92	137.26	81.67	125.55	75.66

Table 6. The rates between Cycle-maximum and Cycle-average values for heat transfer coefficient and heat flux

Excess air ratio λ	Cycle maximum / Cycle average					
	Assanis		Hohenberg		Woshcni	
	h_g	\dot{Q}	h_g	\dot{Q}	h_g	\dot{Q}
3.5	6.58	14.23	6.73	13.45	11.06	20.27
4.0	6.31	13.87	6.65	13.35	10.49	20.11
4.5	6.05	13.33	6.56	13.16	9.81	19.40
5.0	5.78	12.76	6.45	12.86	9.11	18.57

Table 7. The maximum order of magnitudes in heat transfer coefficients

Rate expression	Stroke	Excess air ratio (λ)			
		3.50	4.00	4.50	5.00
$(h_{g,woschni} / h_{g,assanis})_{\max}$	Intake	3.22	3.22	3.22	3.22
	Compression	3.14	3.14	3.15	3.15
	Combustion& Expansion	6.39	6.03	5.72	5.35
	Exhaust	3.91	3.82	3.74	3.69
	Intake	1.34	1.34	1.34	1.34
$(h_{g,woschni} / h_{g,hohenberg})_{\max}$	Compression	0.59	0.59	0.59	0.59
	Combustion& Expansion	1.69	1.55	1.42	1.30
	Exhaust	1.26	1.27	1.27	1.28